Correlated Quantum Phenomena in the Strong Spin-Orbit Regime

William Witczak-Krempa,[1] Gang Chen,[2] Yong Baek Kim,[3,4] and Leon Balents[5]

[1]Perimeter Institute for Theoretical Physics, Waterloo, Ontario N2L 2Y5, Canada

[2]Department of Physics, University of Colorado, Boulder, Colorado 80309-0390

[3]Department of Physics, University of Toronto, Toronto, Ontario M5S 1A7, Canada; email: ybkim@physics.utoronto.ca

[4]School of Physics, Korea Institute for Advanced Study, Seoul 130-722, Korea

[5]Kavli Institute of Theoretical Physics, University of California, Santa Barbara, California 93106

Annu. Rev. Condens. Matter Phys. 2014. 5:57–82

First published online as a Review in Advance on December 20, 2013

The *Annual Review of Condensed Matter Physics* is online at conmatphys.annualreviews.org

This article's doi:
10.1146/annurev-conmatphys-020911-125138

Keywords

spin-orbit coupling, electron correlation, Mott insulator, spin-orbital entanglement, topological insulator, Weyl semimetal, axion insulator, pyrochlore iridates, quantum spin liquid, multipolar order, honeycomb-lattice iridates, double perovskites

Abstract

We discuss phenomena arising from the combined influence of electron correlation and spin-orbit coupling (SOC), with an emphasis on emergent quantum phases and transitions in heavy transition metal compounds with 4*d* and 5*d* elements. A common theme is the influence of spin-orbital entanglement produced by SOC, which influences the electronic and magnetic structure. In the weak-to-intermediate correlation regime, we show how nontrivial band-like topology leads to a plethora of phases related to topological insulators (TIs). We expound these ideas using the example of pyrochlore iridates, showing how many novel phases, such as the Weyl semimetal, axion insulator, topological Mott insulator, and TIs, may arise in this context. In the strong correlation regime, we argue that spin-orbital entanglement fully or partially removes orbital degeneracy, reducing or avoiding the normally ubiquitous Jahn-Teller effect. As we illustrate for the honeycomb-lattice iridates and double perovskites, this leads to enhanced quantum fluctuations of the spin-orbital entangled states and the chance to promote exotic spin liquid and multipolar ordered ground states. Connections to experiments, materials, and future directions are discussed.

1. INTRODUCTION

The subject of this review is the combination of two central threads of quantum materials research. The first, correlated electron physics, is a venerable but still vibrant subject, born from observations of Mott, Hubbard, Anderson, and others on the properties of 3*d* transition metal oxides. It is largely concerned with the diverse properties of electronic materials that are insulating, or in the process of becoming so, as a result of electron-electron interactions (1, 2), most importantly the strong local Hubbard repulsion U between electrons that occupy the same orbital. A plethora of phenomena arises from correlated electron physics, including local moment formation and magnetism, correlated metallic states, quantum criticality, and unconventional superconductivity (2). The second thread of quantum materials research, nontrivial physics from strong spin-orbit coupling (SOC), includes a body of work on *f*-electron materials (3) and the much more recent activity that began with the theoretical proposal of topological insulators (TIs) in 2005 (4–6). SOC is a relativistic effect that provides an interaction between the orbital angular momentum and electron spin in atoms, and is usually considered a small perturbation in the discussion of electrons in solids. However, in heavy elements it need not be weak—it effectively increases proportionally to Z^4, where Z is the atomic number—and indeed has striking qualitative effects. Since 2005, the investigation of topological aspects of electron bands has exploded, both theoretically and experimentally (4–6). From the materials perspective, the domain of the TI field has mostly been the class of solids with heavy *s*- and *p*-electron elements, such as Bi, Pb, Sb, Hg, and Te. In these materials, topologically protected Dirac-like surface states have been predicted and observed, and a host of further phenomena are currently under intense investigation.

The two research strands come together in the heavy transition metal compounds drawn especially from the 5*d* series and, in some cases, the 4*d* series as well. Upon descending the periodic table from the 3*d* to the 4*d* to the 5*d* series, there are several competing trends. First, the *d* orbitals become more extended, tending to reduce the electronic repulsion U and thereby diminish correlation effects. However, simultaneously, the SOC increases dramatically, leading to enhanced splittings between otherwise degenerate or nearly degenerate orbitals and bands, in many cases reducing the kinetic energy. The latter effect can offset the reduction in U, allowing correlation physics to come into play.

It is instructive to consider a generic model Hamiltonian that describes the above discussion:

$$H = \sum_{i,j;\alpha\beta} t_{ij,\alpha\beta}\, c^{\dagger}_{i\alpha} c_{j\beta} + \text{h.c.} + \lambda \sum_{i} \boldsymbol{L}_i \cdot \boldsymbol{S}_i + U \sum_{i,\alpha} n_{i\alpha}(n_{i\alpha} - 1)\,, \qquad 1.$$

where $c_{i\alpha}$ is the annihilation operator for an electron in orbital α at site i, $n_{i\alpha} = c^{\dagger}_{i\alpha} c_{i\alpha}$ is the corresponding occupation number, t is the hopping amplitude, λ is the atomic SOC entangling spin ($\boldsymbol{S}_i$) and angular momentum ($\boldsymbol{L}_i$), and U is the Hubbard repulsion. An explicit example of the spin-orbital entanglement due to λ is given later in Equation 3. We have for simplicity omitted the Hund's interaction between spins in different orbitals on the same site, which is much smaller than U but can sometimes have significant effects (7); however, it is unimportant in the specific examples discussed in detail in this review. A schematic phase diagram can be drawn as in **Figure 1** in terms of the relative strength of the interaction U/t and the SOC λ/t (8). We emphasize this is schematic, in part because the problem is unsolved and in part because Equation 1 can represent many different physical situations by the choice of orbitals and lattice and band structure encoded in $t_{ij,\alpha\beta}$, and the ground states that occur certainly depend on these choices. In this diagram, two lines (which are not meant necessarily as sharp boundaries but rather as demarcating different limits) divide the

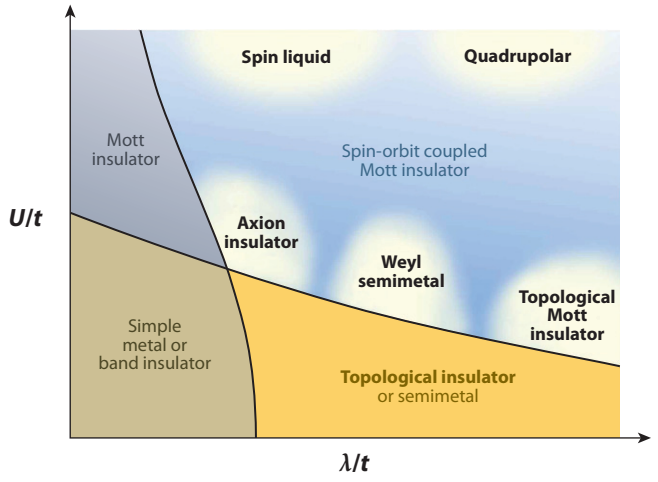

Figure 1

Sketch of a generic phase diagram for electronic materials in terms of the interaction strength U/t and spin-orbit coupling λ/t. The phases described in this review (*bold text*) reside on the right half of the figure.

weak and strong correlation regions and the weak and strong SOC regimes, thereby generating four quadrants. Conventional transition metal materials reside on the left-hand side of the diagram, where SOC is weak $\lambda/t \ll 1$, and a conventional metal-insulator transition (MIT) may occur when U is comparable to the bandwidth, i.e., a few times t. Upon increasing SOC, when $U/t \ll 1$, a metallic or semiconducting state at small U may be converted to a semimetal or to a TI. What happens when both SOC and correlations are present? Several arguments suggest that, in generating insulating states, λ and U tend to cooperate rather than compete. Including SOC, we have already remarked upon the splitting of degeneracies and the consequent generation of multiple narrow bands from relatively mixed bands. The narrow bands generated by SOC are more susceptible to Mott localization by U, which implies that the horizontal boundary in **Figure 1** shifts downward with increasing λ. If we include correlations first, the U tends to localize electrons, diminishing their kinetic energy. Consequently the on-site SOC λ, which is insensitive to or even reduced by delocalization, is relatively enhanced. Indeed, in the strong Mott regime $U/t \gg 1$, one should compare λ with the spin exchange coupling $J \propto t^2/U$ rather than with t. As a result, the vertical boundary shifts to the left for large U/t. We see that there is an intermediate regime in which insulating states are obtained only from the combined influence of SOC and correlations—these may be considered spin-orbit-assisted Mott insulators. Here we are using the term Mott insulator to denote any state that is insulating by virtue of electron-electron interactions. In Section 4, we remark briefly on a somewhat philosophical debate as to what should properly be called a Mott insulator.

Terminology aside, an increasing number of experimental systems have appeared in recent years in this interesting correlated SOC regime. A collection of iridates has received special interest. These are weakly conducting or insulating oxides that contain iridium, primarily found in the Ir^{4+} oxidation state. This includes a Ruddlesden-Popper sequence of pseudocubic and planar perovskites [$Sr_{n+1}Ir_nO_{3n+1}$ ($n = 1, 2, \infty$)] (9–16), hexagonal insulators [$(Na/Li)_2IrO_3$] (17–22), a large family of pyrochlores ($R_2Ir_2O_7$) (23–25), and some spinel-related structures (26, 27). Close to iridates in the periodic table are several osmium oxides, such as $NaOsO_3$ (28) and $Cd_2Os_2O_7$ (29), which experimentally display MITs. Apart from these materials where the microscopic SOC

is strong ($\lambda \approx 0.4$eV), there are also examples that arise in materials near the top of **Figure 1** in which electrons are strongly localized, causing the competing exchange scale to be anomalously weak, making even smaller SOC strong. This includes the spin-orbital liquid material $FeSc_2S_4$ (30–32), possibly the single-layer vanadate Sr_2VO_4 (144, 145), and a host of double perovskites, $A_2BB'O_6$ (33–46), where the exchange scale is small because the electronically active B' ions are spatially well separated. For space reasons, we cannot discuss all of these materials, but we do take examples from this list as illustrations.

This review is organized on the basis of a consideration of two limits within this domain: the weak-to-intermediate correlation regime $U/W \lesssim 1$, where W is the bandwidth that is typically a few times t, and the strong Mott limit $U/W \gg 1$. Both are found in the presence of strong SOC. Conceptually, in the former, the electrons remain delocalized enough that band or band-like topology continues to play an important role, as in the case of TIs (4–6). Notably, interactions open up possibilities for new types of topological phases. This includes Weyl semimetals (WSMs) with Dirac-like bulk quasiparticles and surface Fermi-arc states (47–49, 64) and axion insulators with unusual electromagnetic responses (50, 51), which can arise in the presence of spontaneous magnetic order. Phase transitions between these states (8, 47–52) and among metals and insulators also occur in this regime, and yet more exotic phases have also been envisioned (8, 53). We discuss this weak-to-intermediate correlation regime in Section 2, taking the pyrochlore iridates $R_2Ir_2O_7$ as primary experimental examples.

In the strong Mott regime, discussed in Section 3, electron band topology no longer plays a role because the electronic states are not extended. However, SOC still offers new physics by fully or partially lifting orbital degeneracy of partially filled d shells, not by ordering orbitals but by entangling the orbital and spin degrees of freedom (32, 54, 55). This provides a distinct mechanism to avoid the Jahn-Teller effect and classical orbital ordering. The orbital degeneracy may be fully lifted by SOC, which occurs in iridates in the strong Mott+SOC limit, or partially lifted, which is the case for many d^1 or d^2 ions. In this review, we illustrate both possibilities, using the honeycomb iridates (17–22) Na_2IrO_3 and Li_2IrO_3 as examples of the former and double perovskites (33–46) as examples of the latter. In either case, the strong SOC results in strongly anisotropic exchange interactions, and for the case of partial degeneracy lifting, these have a highly nontrivial multipolar nature (54, 55). We describe how these unusual interactions can promote large quantum fluctuations and lead to novel quantum ground states that are not possible without strong SOC (54–56). In particular, quantum spin liquid and quadrupolar (spin-nematic) ordered phases have been suggested to occur in these systems.

Table 1 summarizes the emergent phases encountered in this review. The theoretical and experimental status of the weak-to-intermediate and strong correlation regimes are presented in Sections 2 and 3, respectively. We conclude the review with a discussion of open issues and other materials in Section 4.

2. WEAK-TO-INTERMEDIATE CORRELATIONS

Following the discovery of TIs (4, 5), it is now recognized that SOC is an essential ingredient in forming certain topological phases. The TI is characterized by a $\mathbb{Z}_2$ topological invariant, which may be obtained from the band structure, in the presence of time-reversal symmetry (TRS). This phase has a bulk excitation gap but is distinguished from trivial band insulators by the presence of protected metallic surface states. The nontrivial bands in the TI must unwind upon crossing the interface with a time-reversal preserving vacuum or a trivial band insulator, leading to the closing of the excitation gap and a conducting state at the interface. Stemming as it does from band structure considerations, the TI relies upon some degree of itineracy. Other TI-related phases with gapless nodes—point Fermi surfaces—in the bulk have also been explored theoretically and obviously also require delocalized electronic states.

Table 1 Emergent quantum phases in correlated spin-orbit coupled materials[a]

Phase	Symmetry	Correlation	Properties	Proposed materials
Topological insulator	TRS	W-I	Bulk gap, TME, protected surface states	Many
Axion insulator	P	I	Magnetic insulator, TME, no protected surface states	$R_2Ir_2O_7$, $A_2Os_2O_7$
Weyl semimetal	TRS or P (not both)	W-I	Dirac-like bulk states, surface Fermi arcs, anomalous Hall effect	$R_2Ir_2O_7$, $HgCr_2Se_4$, ...
LAB semimetal	Cubic + TRS	W-I	Non-Fermi liquid	$R_2Ir_2O_7$
Chern insulator	Broken TRS	I	Bulk gap, QHE	Sr[Ir/Ti]O_3, $R_2[B/B']_2O_7$
Fractional Chern insulator	Broken TRS	I-S	Bulk gap, FQHE	Sr[Ir/Ti]O_3
Quantum spin liquid	Any	S	Several possible phases, charge gap, fractional excitations	$(Na,Li)_2IrO_3$, Ba_2YMoO_6
Multipolar order	Various	S	Suppressed or zero magnetic moments, exotic order parameters	$A_2BB'O_6$

[a]All phases have U(1) particle-conservation symmetry, i.e., superconductivity is not included. [*A*/*B*] in a material's designation signifies a heterostructure with alternating *A* and *B* elements.
Abbreviations: (F)QHE, (fractional) quantum Hall effect; I, intermediate (e.g., requiring magnetic order but mean-field-like); I-S, intermediate-strong; LAB, Luttinger-Abrikosov-Beneslavskii (94); P, inversion (parity); S, strong; TME, topological magnetoelectric effect; TRS, time-reversal symmetry; W-I, weak-intermediate.

In this section, we discuss phenomena involving band-like topology in the presence of interactions. Nontrivial band topology can probably only arise when correlations are not so strong as to localize electrons fully to single atoms. Consequently, we focus on this regime of weak-to-intermediate correlations. From the theoretical point of view, this means that a Hubbard model, rather than one of localized spins, is likely a better starting point.

What new phenomena can be expected relative to the uncorrelated *s*- and *p*-electron materials that are the mainstay of TI experiments? TIs are obviously stable to interactions, and, quantitatively, correlations may even increase the gap in some cases [with correlations, in contrast to the free case, the surface states have the potential to spontaneously break TRS or even to exhibit exotic fractionalization (146–149)]. A more qualitatively novel prospect is to probe topological phases with spontaneous time-reversal breaking because magnetism is common in correlated materials. In general, the $\mathbb{Z}_2$ classification fails for time-reversal broken systems, and instead Chern insulators, i.e., materials with quantized Hall effects, may occur. In the presence of crystalline symmetries, notably inversion, a $\mathbb{Z}_2$ index may reappear (47, 57–60, 150). This is the case in the axion insulator (47, 58, 59), which is characterized by a quantized magnetoelectric effect, i.e., an electric polarization, $\boldsymbol{P}$, can be generated by applying a magnetic field, $\boldsymbol{B}$: $\boldsymbol{P} = \frac{\theta}{(2\pi)^2}\boldsymbol{B}$, with $\theta = \pi$ such that the ratio *P*/*B* is universal and quantized. In fact, the same is true for three-dimensional TIs, and the quantized magnetoelectric effect can be used to define TIs (61) and axion insulators (51, 62, 63) in the presence of interactions.

Nontrivial topology can also appear in gapless phases, such as in the WSM (47, 64). At the level of band theory, a WSM has a Fermi surface consisting of points where only two bands meet linearly (see **Figure 2**). This implies that either TRS or inversion is broken, for otherwise all bands would be twofold degenerate. In this review, we encounter examples arising from a spontaneous breaking of TRS at sufficiently large U. The band touchings of the WSM are three-dimensional analogs of the massless Dirac fermions in clean graphene. However, contrary to the latter, they should be regarded as topological objects—monopoles or hedgehogs in momentum space—because they act as sources of the momentum space Berry flux (47, 64, 65). Consequently, they always come in pairs with opposite chiralities, corresponding to a positive or negative monopole charge, as illustrated in **Figure 2**. An isotropic example of a Weyl fermion is given by the following Bloch Hamiltonian (we take the touching to be at $\boldsymbol{k}_W$):

$$\mathcal{H}(\boldsymbol{k}) = \pm v\left(\delta k_x \sigma_x + \delta k_y \sigma_y + \delta k_z \sigma_z\right), \quad \delta\boldsymbol{k} = \boldsymbol{k} - \boldsymbol{k}_W, \qquad 2.$$

where $\pm$ corresponds to positive/negative chirality and σ_i are the Pauli matrices acting on the space of the two nondegenerate bands that touch at the Weyl point. Because any local perturbation is a combination of Pauli matrices, it can only move the touching in the Brillouin zone (BZ) and not lift it, given that all σ_i already appear in $\mathcal{H}$. As a consequence of the nontrivial bulk topology, the WSM hosts nontrivial surface states on certain boundaries, which take the form of open Fermi arcs (47), as shown in **Figure 2**. This cannot occur in a purely 2D system, just like the existence of an odd number of Dirac fermions in a 2D lattice model, the latter being possible at the surface of a three-dimensional $\mathbb{Z}_2$ TI, circumventing the fermion-doubling theorem (66). In both cases, however, the partner electronic states exist on the opposite surface, which elegantly resolves the apparent paradox. For some further discussion of WSMs, including other realizations (49, 67,

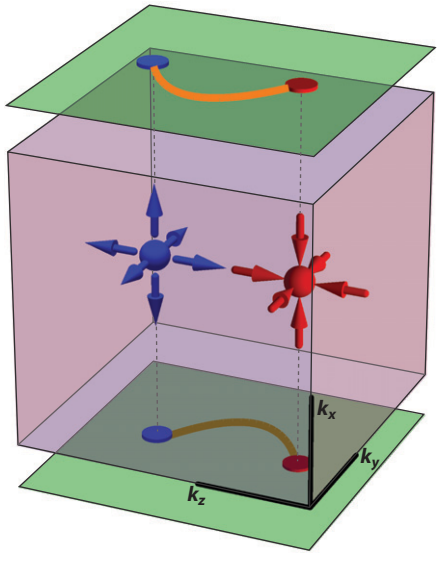

Figure 2

Two opposite-chirality Weyl points in the three-dimensional Brillouin zone (BZ), and the associated Fermi arc surface states. The green sheets correspond to the top and bottom surface-BZs. This minimal Weyl semimetal must break time-reversal symmetry and has a corresponding anomalous quantum Hall conductivity, $\sigma_{xy} = (e^2/2\pi h)\Delta k$, where Δk is the momentum-space separation between the two Weyl points.

68), and of generalizations of these ideas to superconductors (69), we refer readers to recent reviews (70, 71).

The Chern insulator, axion insulator, and WSM require interactions to produce magnetic order, but once produced, a mean-field description in terms of a static exchange field suffices, and the electronic quasiparticles are consequently weakly correlated. Other phases arising in interacting systems with strong SOC may be more intrinsically correlated. Several interacting analogs of TIs have been envisioned that are not adiabatically connected to the ground states of any noninteracting electron Hamiltonian, with or without broken symmetries. These include the topological Mott insulator found in Reference 8, which exhibits spin-charge separation and TI-like surface states composed of neutral fermions, and fractional Chern insulators (72–74), which display a fractional quantum Hall effect without an external magnetic field. Presently, although we believe the ingredients for these sorts of phases are present in the class of materials discussed in this review, a direct connection of specific compounds to specific states of this type is an open theoretical challenge. The final phenomena to be mentioned in the intermediate correlation regime are the thermal and quantum phase transitions. The elephant in the room is the MIT itself, whose character in the strong SOC limit has been little investigated and may be very different from what has been observed in traditional 3*d* compounds. For example, theory has established that the MIT may occur through an intermediate WSM state, and transitions to/from WSM states may be studied. Other types of correlation-driven MITs have been suggested. Note that at $T > 0$, the difference between a metal and an insulator is quantitative not qualitative (because $\sigma \neq 0$ always), so that the evolution from a metal to an insulator at $T > 0$ needs not coincide with any phase transition. The onset of magnetic order in correlated metals and insulators constitutes another type of criticality. Such transitions may again be affected by strong SOC.

2.1. Pyrochlore Iridates

In this section, we expand on the theory and experimental status of new phases and transitions in the context of the pyrochlore iridates $R_2Ir_2O_7$ (R-227), where R is a rare-earth element. We choose these compounds because they constitute a large family for which experiments have revealed thermal phase transitions, an evolution from metallic to insulating behavior, and largely systematic variation of properties with R. Many key theoretical ideas in the field have also been introduced in this context, including topological Mott insulators (8, 53, 151), chiral spin liquids (75), WSMs (47, 48), and axion insulators (47, 51). This has contributed to a substantial experimental effort (23, 24, 76–89) to determine, in particular, the nature of the elusive magnetic ordering. We first review the experimental knowledge of the pyrochlore iridates and then describe the theoret-ical work they have motivated.

2.1.1. Experimental resume. The structure of these materials is well established, consisting of interpenetrating pyrochlore nets for both the rare-earth and iridium ions (23, 90). Each such lattice can be described as a face-centered cubic (fcc) Bravais lattice with four sites per unit cell that form a tetrahedron. The crystal structure is illustrated in **Figure 3**. The fcc lattice constant was found to range from $a = 1.01$ to 1.04 nm (23, 79, 85), depending on the R element. Another important structural parameter is the oxygen x-parameter, which determines the symmetry of the oxygen environment around each Ir cation: When $x = x_{\text{ideal}} = 5/16 = 0.3125$, the oxygens form a perfect octahedron around each Ir. Otherwise, the oxygen octahedron becomes elongated ($x < x_{\text{ideal}}$) or compressed ($x > x_{\text{ideal}}$) along the [111] directions. These distortions are called trigonal because they preserve threefold rotational symmetries. Experiments show that all pyrochlore iridates have compressed octahedra (76, 85).

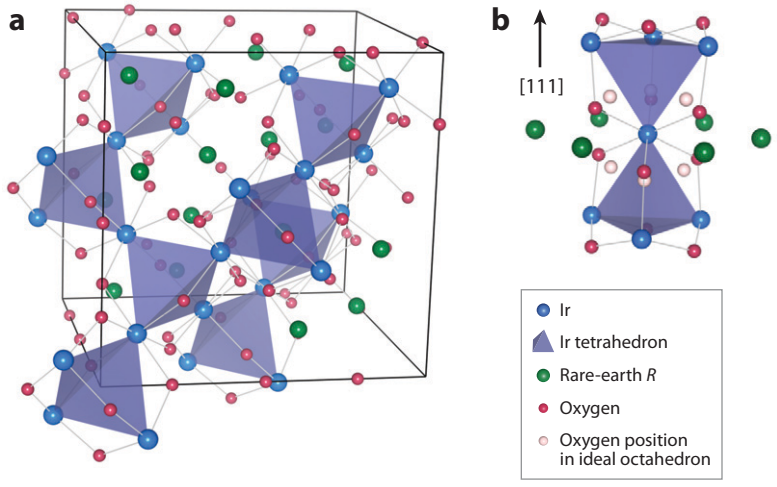

Figure 3

(*a*) Pyrochlore lattice structure showing the Ir tetrahedra. Trigonally compressed cages of oxygens surround each Ir. The box is aligned along the [100], [010], and [001] directions. (*b*) The light spheres correspond to the position of oxygen ions in an ideal octahedron, which is expected for a larger R^{3+} ion. All pyrochlore iridates show trigonal compression of the oxygen cages along the [111] directions.

Let us first review the temperature dependence of the resistivity ρ. All members of the family, except Pr-227, show a diverging ρ at sufficiently low temperature (23, 24, 78). For the compounds with a larger R^{3+} ion, such as Eu-, Sm-, and Nd-227, the resistivity goes from being metallic ($d\rho/dT > 0$) at high temperatures $T > T_c$ to nonmetallic ($d\rho/dT < 0$) at low temperatures $T < T_c$. This is illustrated for Eu-227 in **Figure 4*a***. Pr-227 lies at the end of the spectrum in that it has the largest ionic radius and does not show a major resistivity upturn down to the lowest temperatures, which is in agreement with the above trend. For compounds with smaller R^{3+} ions, such as for $R =$ Lu, Yb, Ho, Y, etc., the slope does not change sign and the resistivity is nonmetallic throughout. In that case, the upturn at T_c is smoother. One can tentatively explain this trend in which a larger R^{3+} cation leads to a more metallic ρ as follows: Larger R^{3+} ions lead to a decreased trigonal compression of the octahedra (**Figure 3*b***), which increases the Ir-O orbital overlap and thus facilitates the hopping of the Ir electrons (91).

A variety of sharp features in the magnetic properties occur at the same temperature as the resistivity upturn, T_c, which supports its interpretation as a true phase transition. Most notably, the field-cooled (FC) and zero field–cooled (ZFC) magnetic susceptibilities branch away from each other (24, 76), as shown in **Figure 4*a*** for Eu-227. In addition, μSR experiments, which have been performed on Eu- (80), Nd- (86, 87), Yb- (88), and Y-227 (88), show the continuous rise of a well-defined muon-precession frequency directly below T_c (illustrated in **Figure 4*a*** for Eu-227). This is indicative of long-range magnetic ordering into a commensurate structure. However, owing to difficulties in performing neutron-scattering experiments on Ir-based compounds, the precise nature of the ordering remains unknown. Nevertheless, it has been inferred that a second-order phase transition to an antiferromagnetic (AF) insulator occurs at T_c. Ferromagnetism can be largely ruled out by the absence of magnetic hysteresis (23, 76). The second-order nature of the transition is further supported by the presence of peaks in the heat capacity at T_c (24, 78). The essence of the experimental observations on the pyrochlore iridates is summarized in the phase diagram in **Figure 4*b***.

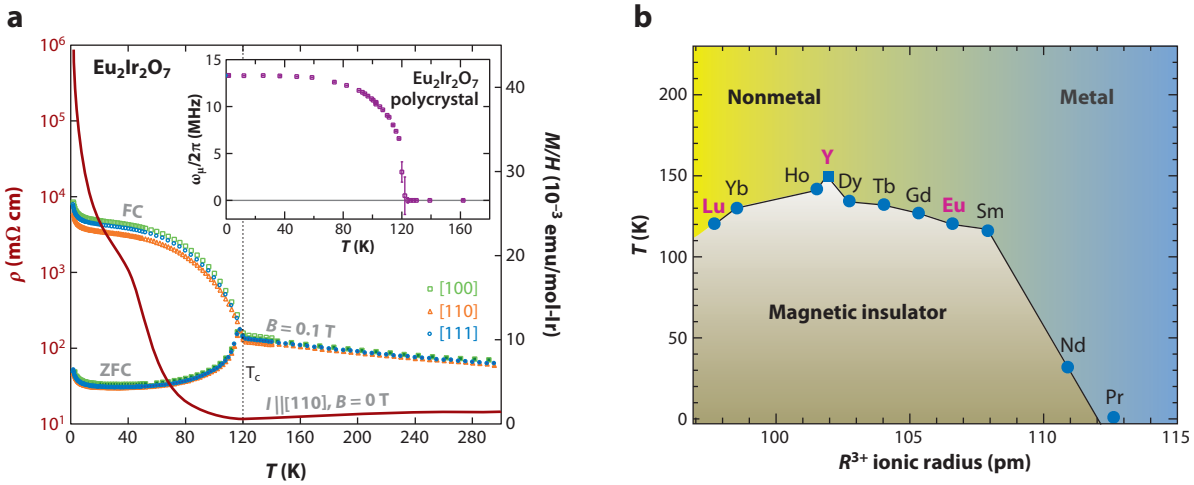

Figure 4

(*a*) The main panel shows the resistivity and field-cooled (FC) and zero field–cooled (ZFC) susceptibilities for Eu-227, and the insert depicts the spontaneous muon oscillation frequency. Data adapted from References 80 and 81. The vertical axis for the susceptibility data represented by green, blue, and orange symbols is on the right. (*b*) Phase diagram for the pyrochlore iridates *R*-227 based on transport and magnetism measurements. This is a supplemented and modified version of the diagram found in Reference 78. The *R*-elements that do not have a local magnetic moment are emphasized in bold magenta. The only non-lanthanide, $R = \mathrm{Y}$, is denoted by a square. Abbreviation: T_c, critical temperature.

2.1.2. Electronic structure. The basic element of the description of these materials is the iridium electronic structure. We neglect for the most part the rare-earth magnetism, which plays a role in some (but not all) of the compounds at very low temperature. Following the analysis of the Ir-electron physics, we briefly examine their interplay with local moments in Section 2.1.5.

We begin by examining the local atomic physics associated with the Ir cations. The outer-shell electrons of Ir^{4+} are in a $5d^5$ configuration, half-filling the ten *d*-levels. The dominant crystal field splitting comes from the oxygen octahedra surrounding each Ir cation, which splits the levels into a higher-energy e_g orbital doublet and a lower t_{2g} orbital triplet, spanned by orbitals with *xy*, *yz*, and *zx* symmetry. These are separated by an ~2 eV gap, and as such we can neglect the higher-energy e_g levels. We then must take into account both the SOC and trigonal distortions. Let us begin with atomic SOC in Ir^{4+} ions. The full angular momentum operator $\boldsymbol{L}$ projected to the t_{2g} manifold acts as an effective angular momentum operator, $\boldsymbol{L}_{\mathrm{eff}}$, up to a minus sign, i.e., $\mathcal{P}_{t2g}\boldsymbol{L}\mathcal{P}_{t2g} = -\boldsymbol{L}_{\mathrm{eff}}$, where $\mathcal{P}_{t2g}$ represents the projection on the t_{2g} manifold. Therefore, the SOC λ splits the t_{2g} spinful manifold into a higher-energy $J_{\mathrm{eff}} = 1/2$ doublet and a lower $J_{\mathrm{eff}} = 3/2$ quadruplet. The states in these multiplets exhibit spin-orbital entanglement. For example, the $J_{\mathrm{eff}} = 1/2$ states are

$$|J^z_{\mathrm{eff}} = +1/2\rangle = \frac{1}{\sqrt{3}}\Big(|xy,\uparrow\rangle + |yz,\downarrow\rangle + i|zx,\downarrow\rangle\Big), \qquad 3.$$

$$|J^z_{\mathrm{eff}} = -1/2\rangle = \frac{1}{\sqrt{3}}\Big(-|xy,\downarrow\rangle + |yz,\uparrow\rangle - i|zx,\uparrow\rangle\Big), \qquad 4.$$

where the up and down arrows indicate the direction of the true spin. In an ionic picture, given that Ir^{4+} has 5 *d*-electrons, the $J_{\mathrm{eff}} = 1/2$ doublet is half-filled, and only this orbital is involved in the low-

energy electronic structure. More generally, if trigonal splitting is included, the $J_{\text{eff}} = 3/2$ levels are split and mixed with the $J_{\text{eff}} = 1/2$ levels. In the general case, there is a highest Kramers doublet, whose character varies with the ratio of SOC to trigonal splitting between a $J_{\text{eff}} = 1/2$ doublet and an $S = 1/2$ doublet.

A band structure view is complementary to the ionic picture, as we now discuss. If only the highest doublet is involved, we expect four twofold degenerate bands near the Fermi energy, as there are four Ir per unit cell. As discussed by Wan et al. (47) and Yang & Kim (52), it is instructive to consider their structure at the Γ point. As a result of cubic symmetry, the eight Bloch states at this point decompose into two two-dimensional irreducible representations (irreps) and one four-dimensional irrep. By electron counting, these bands should be half-filled, so that if the order of these irreps, in terms of degeneracies, is 2-2-4 or 4-2-2, a band insulating state may occur; however, if the order is 2-4-2, the four-dimensional irrep must be half-filled and hence the system cannot be gapped at the band structure level (see the bottom panel in **Figure 5*b***). The former situation was obtained by Reference 8 on the basis of a phenomenological but ad hoc Hubbard model for small U. They found a transition from a semimetallic ground state to a TI state by increasing the ratio of SOC to hopping. Subsequently, by ab initio methods, Wan et al. (47) found the latter (2-4-2) ordering of irreps in Y-227. In this case, a TI is impossible, but other topological phases can occur with increasing correlations. For those iridates with metallic paramagnetic states, the 2-4-2 scenario may be more plausible.

A convenient tight-binding model that covers both limits was introduced in References 48 and 92. It considers the minimal number of degrees of freedom, i.e., a single Kramers doublet per site, which leads to a total of eight bands. One can show that the most general nearest-neighbor TRS Hamiltonian has the form

$$H_0 = \sum_{\langle i,j \rangle} c_i^\dagger (t_1 + i t_2 \boldsymbol{d}_{ij} \cdot \boldsymbol{\sigma}) c_j \qquad 5.$$

(93), where the hopping parameters t_1 and t_2 are real, and $\boldsymbol{\sigma}$ is a vector of Pauli matrices acting on the pseudospin degree of freedom. The t_2 term generates nontrivial Berry phases for the hopping electrons, and plays a key role in realizing topological phases. The real vector $\boldsymbol{d}_{ij}$ is aligned along the opposite bond of the tetrahedron that contains i, j. Diagonalization of H_0 reveals a semimetallic state with the 2-4-2 ordering when $-2 \leq t_2/t_1 \leq 0$, and a TI otherwise, with the exception of a band closing at $t_2/t_1 = 1$ (92, 93). Notably, the semimetallic state so obtained is not a compensated system with electron-hole pockets but a zero-gap semiconductor. More recently, it was argued that such a state forms a stable non-Fermi liquid phase with a quadratic band touching at the Γ point, christened a Luttinger-Abrikosov-Beneslavskii (LAB) phase for historical reasons (94).

2.1.3. Magnetism and Weyl fermions. As discussed in Section 2.1.1, the experimental results strongly suggest AF order in the low-temperature insulating state of the iridates. This is also indicated via theory. Ab initio calculations in the LDA+U framework [it should now be clear that LDA+U stands for a type of ab initio approach. Readers can always find more information in Reference 47] by Wan et al. (47) found an AF ground state with each spin oriented along its local trigonal axis and all spins on a given tetrahedron pointing in or out of that tetrahedron. Such an all-in/all-out (AIAO) state, illustrated in **Figure 5**, maintains the unit cell and cubic symmetry of the lattice and is consistent with the lack of any indication of structural transitions in experiment. The same AIAO state was obtained in a phenomenological Hubbard model by theoretical methods of varying sophistication (48, 51, 92).

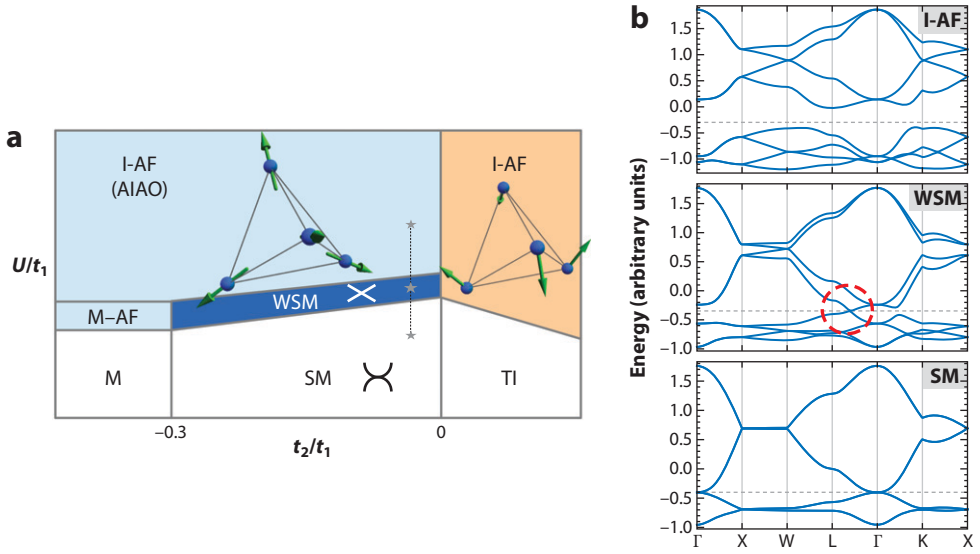

Figure 5

(*a*) Schematic mean-field phase diagram of the Hubbard model on the pyrochlore lattice (48, 92) (the kinetic Hamiltonian, Equation 3, has been supplemented by small next-nearest-neighbor hopping). The shaded regions harbor an antiferromagnetic (AF) order, which can be of the AIAO type (*light blue*) or a related type (*orange*). (*b*) The evolution of the electronic spectrum along the three points (*stars*) highlighted on the vertical dashed line in panel *a*. The red circle shows one Weyl point at the Fermi level (*horizontal dashed line*). The spectrum is plotted along high symmetry lines in the Brillouin zone. Abbreviations: AIAO, all-in/all-out; I-AF, insulating antiferromagnet; M, metal; M-AF, metallic antiferromagnet; SM, semimetal; TI, topological insulator; WSM, Weyl semimetal.

In the magnetically ordered state, the broken TRS but preserved inversion symmetry admits the possibility of both WSM and axion insulator phases. Wan et al. (47) indeed found a WSM phase for a range of U in their LDA+U calculations and suggested but did not find an axion insulator state. In fact, introduction of arbitrarily weak AIAO magnetic order converts the quadratic band–touching LAB phase to a Weyl semimetal (48, 92), which is illustrated in the middle panel of **Figure 5*b***. As remarked earlier, this phase is stable, and indeed the Weyl points must migrate from the Γ point toward the zone boundary to pairwise annihilate before a true insulator is found at larger U. Such behavior was found by adding a Hubbard repulsion U to the tight-binding model of Equation 3 within a Hartree-Fock approximation (48, 92) (small, second-neighbor hopping is needed to obtain the generic linear dispersion relation in the WSM phase with AIAO order). This is illustrated in **Figure 5**. The quantitative width of the WSM in phase space varies between different calculations and can be very narrow, owing to rather flat bands and the relatively fast growth of the local moment as the AIAO phase is entered. Other types of magnetic order, e.g., ferromagnetism, can also induce Weyl points or relatives of Weyl points (94).

Many signatures of the WSM have been suggested. We have already mentioned the surface Fermi arcs. Without disorder, the low-frequency optical conductivity scales as $\sigma(\omega) \sim \omega$. Although a pair of opposite Weyl points mediates an intrinsic Hall conductivity (95), this sums to zero given the cubic symmetry of the AIAO state, which dictates at least eight nodes. However, it has been suggested that zero-field Hall conductivity could be induced by the appropriate strain (95). Interesting transport phenomena related to the Adler-Bell-Jackiw anomaly of Weyl fermions are predicted in parallel electric and magnetic fields (96). In general, taking into

account the interplay of various types of disorder and interactions in the WSM makes modeling transport challenging.

A nice point of consistency of the proposed AIAO magnetic order is that it is characterized on Landau symmetry grounds by a simple Ising order parameter, for which a continuous thermal transition is allowed. As remarked earlier, the thermal MITs indeed appear continuous in the experiments. Adding finite temperature to the simple mean-field Hubbard model calculation further corroborates the expectation from Landau reasoning, showing that the magnetic transition is continuous, and its critical temperature grows with U, following the behavior of the charge-excitation gap (92). It may be interesting to study the corresponding thermal and quantum phase transitions in the future, for which the mean-field analysis may be inadequate.

2.1.4. The role of many-body effects. In the preceding section, we considered correlations only at the mean-field level. This is expected on general grounds to be qualitatively correct for describing many phenomena within the phases so obtained. For example, in fully gapped states, such as the TI or gapped AIAO phase, the gap cannot be broken by any small perturbation. The WSM is also stable to interactions, which are irrelevant (marginally for long-range Coulomb) in the renormalization group sense, although they may have important transport consequences. A cellular dynamical mean-field theory (CDMFT) (97, 98) study bears out the robustness of the mean-field treatment, although it shows that correlations may yet induce new phases: An axion insulator state appears in the CDMFT analysis (51) of Equation 3 (plus Hubbard U), but it does not arise at the Hartree-Fock level. For these calculations, a convenient formulation of the $\mathbb{Z}_2$ topological invariant in terms of the interacting electron Green's function (62) was employed.

Other qualitative effects of correlations exist. Most obviously, it is likely that at least some of the quantum phase transitions indicated in **Figure 5** are not fully captured by mean-field theory. Excitations in the intermediate correlation regime, which may be measured in the future by resonant inelastic X-ray scattering (RIXS) or other methods, may interpolate between the spin-orbital waves of localized electron theory and the random phase approximation collective modes of itinerant electron theory. Of course, neither CDMFT nor the simpler Hartree-Fock theory is capable of capturing the more subtle quantum correlations in other proposed phases, such as the topological Mott insulator, but we do not know that such phases can be found in the iridates.

2.1.5. Interactions with rare-earth moments. We now briefly turn our attention to the interactions between the R-site f-electrons and the Ir d-electrons. Depending on the electronic configuration of the ion R^{3+}, the f-electrons can carry a net magnetic moment in a Kramers doublet (R = Nd, Sm, Gd, Dy, Yb) or a non-Kramers doublet (Pr, Tb, Ho). Generally, if the Ir ions order magnetically, the rare-earth spins must experience an exchange field and also order at low temperature. Given that $4f$ spins are rather highly localized, the exchange coupling between rare-earth and Ir spins is expected to be relatively weak, so the back-reaction on the Ir dynamics is expected to be small. This is consistent with experiments on Yb-227 and Y-227 (88), which show spontaneous local fields in μSR at comparable temperatures ($T_M = 130$ K, 150 K, respectively), although Yb^{3+} carries a net moment and Y^{3+} does not. This is presumably Ir magnetism. Signs of Yb spin ordering or freezing appear only below $T^* \approx 20$ K (88).

Nevertheless, the R spins can have a substantial influence on low-energy properties, and their magnetism may be nontrivial. The most notable example is $Pr_2Ir_2O_7$, which remains metallic to low temperature and shows no clear magnetic ordering transition (99). Instead, novel freezing and non-Fermi liquid phenomena appear at low temperature, apparently driven by Pr magnetism (99). Most strikingly, a zero-field anomalous Hall effect has been observed below 1.5 K despite the absence of magnetic order or freezing for $T > 0.3$ K, leading to the proposal that this is a realization

of a chiral spin liquid (75, 100). Spin-ice type physics for the Pr moments, i.e., predominantly two-in/two-out configurations on each tetrahedron, has also been inferred. Several theoretical works (101–103, 152) have suggested origins for these phenomena, including ordinary and exotic RKKY interactions, quadrupolar ordering, etc. As of this writing, the physics of $Pr_2Ir_2O_7$ remains unresolved. Overall, much less theoretical attention has been paid to the physics of other rare-earths *R*, but one work suggests their coupling to Ir may help to stabilize the WSM and axion insulator phases (104).

2.1.6. Issues and outlook. This section has outlined the theoretical and experimental work on the pyrochlore iridates. Both support a picture of the high-temperature state as a paramagnetic semimetal, possibly a zero-gap semiconductor. The MIT or crossover occurs simultaneously with the onset of commensurate magnetic order, most likely of AIAO type. Although the transport phenomenology in these materials is very complex, and clearly requires more theoretical modeling, the rough behavior of the resistivity is in accord with static and dynamical mean-field-theory results: The onset of the AIAO order generally opens up a charge gap in an otherwise metallic or semimetallic paramagnetic state, and the MIT temperature becomes smaller as the relative correlation strength *U*/*t* gets weaker (92). Understanding low-temperature transport remains a challenge.

A direct determination of the magnetic structure of each member of the series is desirable to confirm or disprove the AIAO for all or some compounds. It has been argued that the AIAO order observed at the Nd sites in Nd-227 provides indirect evidence for the AIAO at the Ir sites, as the ordering at Nd sites may be caused by an effective field from the Ir sites (82). Recent standard and resonant X-ray diffraction measurements on Eu-227 (89) find $\boldsymbol{q} = 0$ magnetism with no indication of any lowering of lattice symmetry, prompting the authors of Reference 89 to suggest that it must be the AIAO AF.

We have focused primarily on possible electronic phases, but it is also important to understand various experimental observables. In particular, the excitation spectrum of the insulating and conducting states should be determined. An understanding of the effects of disorder and interactions on Weyl fermions is demanded to confront spectroscopic studies. As an example, the optical conductivities of Nd-227 and Rh-doped Nd-227 were recently measured (105). The optical conductivity of Nd-227 has a striking charge gap, whereas Rh-doped Nd-227 shows low-energy spectral weight that may be interpreted as evidence for a WSM (although in our opinion many other explanations are possible for the latter) (105). There should also be collective magnetic excitations (magnons) and possibly excitons, which may be studied by RIXS (11–16) or other techniques. Theoretical calculations of both optics (92) and magnetic excitations (106) already exist for the phenomenological Hubbard model given in this review. Direct examination of surface states by photoemission or tunneling is challenging but of great interest.

3. STRONG MOTT REGIME

In this section, we consider strong Mott insulators, by which we mean materials for which it is sufficient to regard electrons as being localized effectively to single atoms, and that consequently admit a description in terms of local spin and orbital degrees of freedom. This requires a priori that the charge gap is large compared with the energy of spin and orbital excitations. In reality, spin-orbital exchange Hamiltonians may also provide an intuitive description of some phenomena even in intermediate correlation situations, where charge fluctuations are significant. We do not comment further on this and proceed with the strong Mott discussion.

The role of strong SOC in the strong Mott regime is clearly very different than that in more itinerant systems because if electrons can be regarded as wholly localized, then considerations of

band topology do not apply. In the strong Mott regime, the interesting physics of SOC arises from the unique way in which it—wholly or partially—resolves orbital degeneracy. Orbital degeneracy is germane to correlated materials in which the environment of transition metal atoms often has at least approximate octahedral or tetrahedral symmetry, resulting in degenerate doublets or triplets of orbitals. When these shells are neither half-filled nor full, orbital degeneracy arises. In principle, even without SOC, this leads to interesting physics in which the orbital degree of freedom behaves as an additional pseudospin quantum variable. The combined exchange of spin and pseudospin is given then by Kugel-Khomskii models (107). In practice, the quantumness of the orbitals is usually compromised by the Jahn-Teller effect, in which lattice distortions spontaneously arise to split the orbital degeneracy (108). Even at temperatures above this orbital ordering temperature, the associated phonon modes couple strongly to the orbital pseudospin, damping and decohering it. Consequently, a sadly mundane reduction of the beautiful Kugel-Khomskii Hamiltonian, by simply replacing the orbital pseudospin with its classical expectation value, seems to be adequate for the description of many orbitally degenerate transition metal systems, such as perovskite manganites. Even in the rare situations in which something more subtle is suspected, the mixing of orbital and lattice modes makes it practically difficult to clearly distinguish collective orbital excitations in experiments.

SOC offers a more interesting way of resolving orbital degeneracy: trading the Jahn-Teller effect for the entanglement of spin and orbital degrees of freedom. It may entirely suppress the orbital degeneracy, leaving behind a pure Kramers doublet, as in the case of the $J_{\rm eff} = 1/2$ states of Ir^{4+} ions, or even selecting a spin-orbital singlet state for some non-Kramers ions, as in the case of tetrahedral Fe^{2+} (32). In other cases, the degeneracy lifting may be partial, leading to effectively larger spin-orbital pseudospins. In either the Kramers or the latter case, the interactions among the remaining highly entangled states are strongly affected by this entanglement and the underlying spin-orbital exchange. Consequently, not only do such systems (at least largely) avoid the Jahn-Teller effect, but they enjoy exotic exchange interactions that foster unusual ground states. In the remainder of this section, we discuss, in particular, the possibilities of quantum spin liquid and multipolar ordered phases as well as unconventional magnetically ordered states. We illustrate these possibilities through two material examples, the honeycomb iridates and the double perovskites.

3.1. Full Degeneracy Lifting and Honeycomb Iridates

As discussed already in Section 2.1.2, for an octahedrally coordinated Ir^{4+} ion with $5d^5$ configuration, SOC completely removes orbital degeneracy, resulting in a maximally quantum effective spin-1/2 Hamiltonian, representing the $J_{\rm eff} = 1/2$ states. One can say that the orbital degeneracy is fully lifted, with the remaining degeneracy being guaranteed by Kramers theorem. The hexagonal iridates Na_2IrO_3 and Li_2IrO_3, which realize a layered structure consisting of a honeycomb lattice of Ir^{4+} ions, provide a concrete example of this case. Both compounds appear to be in the strong Mott regime. As shown by Jackeli & Khaliullin (109) in the ideal limit, the edge-sharing octahedral structure and the structure of the entangled $J_{\rm eff} = 1/2$ orbitals lead to a cancellation of the usually dominant AF oxygen-mediated exchange interactions. A subdominant term is generated by Hund's coupling, which takes the form of a highly anisotropic exchange:

$$H_K = -K \sum_{\alpha=x,y,z} \sum_{\langle ij\rangle \in \alpha} S_i^\alpha S_j^\alpha, \qquad 6.$$

where $\mathbf{S}_i$ are the effective spin-1/2 operators, and $\alpha = x, y, z$ labels spin components and the three orientations of links on the honeycomb lattice. This peculiar and highly frustrated Hamiltonian is,

remarkably, nearly the only example of an exactly soluble model for a quantum spin liquid state. As shown in an ingenious and tour de force paper by Alexei Kitaev (110), Equation 6 describes a state with no magnetic order and with elementary excitations that are charge-neutral spin-carrying Majorana fermions that are their own antiparticles. It is astonishing that the Kitaev exchange form of Equation 4, which is very unnatural for conventional magnetic systems, arises organically from the geometry and entanglement in the strong SOC limit.

The experimental situation is more complex. In this (111, 112) and other (113) contexts, it has been argued that an isotropic Heisenberg interaction is generated from the direct overlap of $5d$ orbitals. The resulting Heisenberg-Kitaev model has been studied by several methods that demonstrate that with increasing Heisenberg coupling the ground state undergoes successive transitions from the Kitaev spin liquid to a stripy four-sublattice magnetically ordered state and to the usual two-sublattice magnetically ordered state. Recent neutron-scattering experiments and other studies show that the ground state of Na_2IrO_3 is, however, none of these states, but instead displays a different collinear magnetic order, the so-called zigzag state with a four-sublattice structure (20, 22). This has generated a number of new theoretical proposals to explain the apparent departure from the Heisenberg-Kitaev model (114–118). Possibly important ingredients to explain the experiments are other symmetry-allowed interactions on nearest-neighbor bonds, which might emerge from trigonal crystal fields or other mechanisms and exchange with second and third neighbor sites. However, it has been suggested that the Kitaev interaction might be much larger in Li_2IrO_3, and the system may be closer to the quantum spin liquid phase (18). It is perhaps worthwhile to comment on the role of frustration. Often in antiferromagnets, SOC, e.g., via the Dzyaloshinskii-Moriya interaction, is thought to remove accidental degeneracy and favor order. The Kitaev model is a counterexample, showing that in some cases strong SOC can suppress ordering. However, one should be aware of both possibilities.

3.2. Partial Degeneracy Lifting and Ordered Double Perovskites

In other situations, SOC may reduce but not fully eliminate the orbital degeneracy. Such partial degeneracy removal still has dramatic effects upon the physics. As an example, we consider a family of compounds with one or two electrons in the $4d$ or $5d$ shell. These are thus moderately to strongly spin-orbit coupled analogs of the well-studied $3d$ titanates with Ti^{3+} and vanadates with V^{3+} or V^{4+} states. The latter materials constitute classic families undergoing Mott transitions (1). In octahedral coordination and for vanishing SOC, these valence states possess a threefold orbital degeneracy and consequently are Jahn-Teller active in the solid and tend to exhibit complex orbitally ordered states.

When SOC is dominant, we can understand the partial degeneracy lifting as follows. The t_{2g} orbitals split just as in iridates, but with the one or two electrons now occupying the $J_{\text{eff}} = 3/2$ quadruplet. In the d^1 case, this simply results in a $J_{\text{eff}} = 3/2$ local effective spin. In the case of the d^2 electron configuration, the description based solely on single-particle states no longer holds, but the result is similar. Following Hund's rules applied to the d^2 configuration, one finds a total spin, $S = 1$, and an effective orbital angular momentum (threefold degeneracy), $L_{\text{eff}} = 1$. In the end S and L align so that an effective $J_{\text{eff}} = 2$ spin results when SOC is included (55, 119). We see that in both cases the ionic degeneracy (= 4 and 5 for d^1 and d^2, respectively) is reduced from that without SOC (= 6 and 9, respectively) but is still larger than what is required by Kramers theorem alone (= 2 and 1, respectively).

What physics can we expect from the effective spins? Large spins, such as $S = 3/2$, 2, etc., are often thought to behave relatively classically. This is based on the standard spin-wave expansion for Heisenberg-type models, which indeed can be cast as an expansion in $1/S$. However, the classicality of such spins in fact depends critically on the nature of their interactions. Many

examples of nonclassical behavior for larger spins can be found in the theoretical literature, notably spin-nematic or quadrupolar ordered phases of spin-one systems with biquadratic exchange (120), Haldane type states for $S \geq 1$ Affleck-Kennedy-Lieb-Tasaki (AKLT) models (121), and quantum spin liquid states of large N $SU(N)$ and $Sp(N)$ antiferromagnets (122). All these cases can be cast in the form of models in which spins with $S > 1/2$ interact with higher-order exchange interactions that involve multiple spin operators on each site (but typically with spins still interacting pairwise). One can describe such interactions as consisting of coupling between multipole moments (beyond dipoles) of the spins. Heuristically, multipolar interactions enhance quantum fluctuations because they directly connect states with very different S^z quantum numbers, allowing the wave function to easily delocalize in the spin space. By contrast, the usual bilinear Heisenberg interactions induce only single spin flips, and consequently tend to localize the spin-wave function near some classical extremum.

Unfortunately, multipolar interactions are very weak in conventional systems with weak SOC. However, this is not true for the effective spins in the strong SOC limit. This is because spin exchange is always dependent on the orbital state, and in the strong SOC limit, spins and orbitals are highly entangled. This entanglement transfers the orbital dependence of the exchange to the effective spin, generating multipolar exchange, as explained in Section 3.2.2. Thus, for spin-orbitally entangled effective spins, strong multipolar exchange is generic. We illustrate this in the following subsections for one class of materials.

3.2.1. Double perovskites. For numerous examples of partially quenched degeneracy of the above type, we turn to the double perovskite materials $A_2BB'O_6$, whose structure is shown in **Figure 6*a***. It can be derived from the simpler cubic perovskite structure ABO_3 by replacing the single B atom with alternating B and B' atoms on two rock-salt sublattices. There are many such compounds with nonmagnetic B sites and B' sites occupied by the 4*d* and/or 5*d* transition metal elements with d^1 or d^2 configuration. Because of the difference in the valence charges and ionic radius between B and B' ions, the magnetic B' ions form an fcc lattice structure with very little intersite disorder and a lattice constant twice that of the original cubic case. As shown in **Table 2**, the magnetic ions B' (Re^{6+}, Os^{7+}, and Mo^{5+} for d^1; Re^{5+} and Os^{6+} for d^2) have one or two electrons on the 4*d* or 5*d* shell (33–46). Like iridium, such heavy elements and high orbital shells naturally incorporate strong SOC. Moreover, the large separation of the metal ions in this structure suppresses electron hopping and promotes Mott-insulating behavior.

Immediate evidence for orbital degeneracy lifting can be found in several of these materials. One consequence of the strong SOC limit is a reduction of the effective moment. In fact, for the $J_{\text{eff}} = 3/2$ state in an ideal isolated ion, the orbital and spin contributions cancel, and the moment vanishes, i.e., the *g*-factor is zero. As a result of mixing with neighboring oxygen ions, the magnetic moment is generally nonzero in the solid, but a small *g*-factor is still expected. The situation for $J_{\text{eff}} = 2$ is similar but less dramatic: The magnetic moment is reduced to $\boldsymbol{M} = \boldsymbol{S}_{\text{eff}}/2$, i.e., $g = 1/2$. Indeed, the magnetic moments of most compounds in **Table 2** are smaller than the values expected from a spin-only contribution, which is consistent with the effective local moment renormalized by the strong SOC (54, 55, 123, 124).

Another indicator of strong SOC is the magnetic entropy, which can give direct evidence of the quadruplet or quintuplet structure. In Ba_2YMoO_6, an entropy of $R \ln 4$ (here R is the gas constant) was indeed estimated from integration of the magnetic specific heat (34), which is consistent with the $J_{\text{eff}} = 3/2$ state.

3.1.2. Multipolar exchange. We now explain how multipolar exchange arises from spin-orbital entanglement, a known phenomenon in *f*-electron systems (3). The basic idea is to consider the

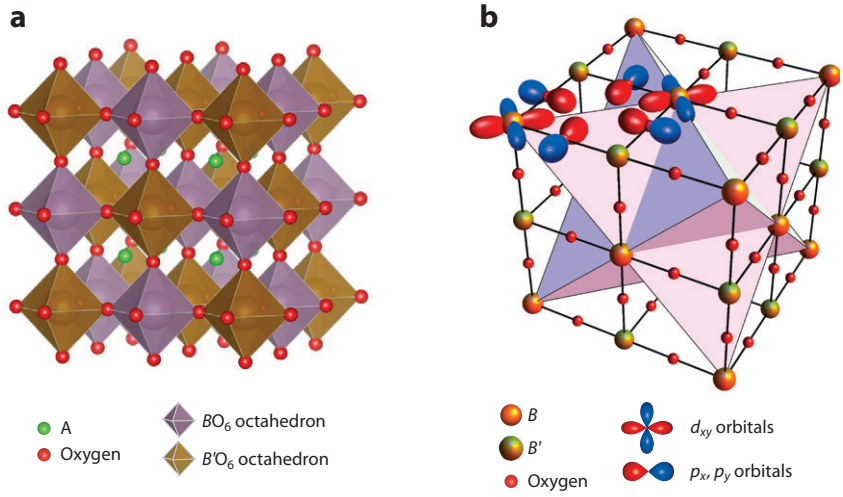

Figure 6

(*a*) The crystal structure of an ordered double perovskite, $A_2BB'O_6$. (*b*) The same structure, showing the representation of the geometrically frustrated fcc lattice of *B* sites as edge-sharing tetrahedra. Two d_{xy} orbitals on nearest-neighbor *B* sites are shown with the intermediate p_x, p_y orbitals involved in their exchange path. *A* sites are not shown.

Kugel-Khomskii-type exchange that arises when all orbitals are included, and then to project that exchange to the effective spins that form in the strong SOC limit. In general, several different exchange processes contribute to the appropriate Kugel-Khomskii model for double perovskites. For simplicity, we illustrate only one in detail here and refer the reader to References 54 and 55 for more detail. We consider the d^1 case and focus on the nominally AF nearest-neighbor processes via intermediate oxygens, which are expected to dominate. These processes are strongly restricted by orbital degrees of freedom. As is illustrated in **Figure 6*b***, in *xy* planes only electrons residing on d_{xy} orbitals can virtually transfer to neighboring sites via p_x and p_y orbitals of the intermediate oxygens (the same process may be understood as a direct exchange between molecular orbitals consisting of transition metal d_{xy} and neighboring oxygen *p* levels). Therefore, the AF exchange interaction can be written as $\mathcal{H}_{\rm ex} = \mathcal{H}^{xy}_{\rm ex} + \mathcal{H}^{yz}_{\rm ex} + \mathcal{H}^{xz}_{\rm ex}$ with

$$\mathcal{H}^{xy}_{\rm ex} = J \sum_{\langle ij\rangle \in xy \text{ plane}} \left(\boldsymbol{S}_{i,xy} \cdot \boldsymbol{S}_{j,xy} - \frac{1}{4} n_{i,xy} n_{j,xy} \right), \qquad 7.$$

where the sum is over nearest-neighbor sites in the *xy* planes, and the corresponding terms in *yz* and *xz* planes are obtained by a cubic permutation. Here the operators $\boldsymbol{S}_{i,xy}$ and $n_{i,xy}$ denote the spin residing on the d_{xy} orbital and d_{xy}-orbital occupation number, respectively, at site *i*.

Without SOC, and as written, the above interaction appears relatively conventional and, in particular, is bilinear in $\boldsymbol{S}_{i,xy}$. However, this can be rewritten by explicitly representing the orbital degree of freedom via the effective $L = 1$ angular momentum $\boldsymbol{L}$ describing the t_{2g} degree of freedom. One has $\boldsymbol{S}_{i,xy} = \boldsymbol{S}^{\rm tot}_i \left[1 - (L^z_i)^2 \right]$ and $n_{i,xy} = 1 - (L^z_i)^2$, where $\boldsymbol{S}^{\rm tot}_i = \boldsymbol{S}_{i,xy} + \boldsymbol{S}_{i,xz} + \boldsymbol{S}_{i,yz}$ is the total true spin on site *i*. With these substitutions, we see that up to three spin or pseudospin operators are multiplied on each site *i* or *j*. In the strong SOC limit, i.e., $J \gg \lambda$, this should be projected onto the $J_{\rm eff} = 3/2$ effective spin. That is, we should replace $\mathcal{H} \to \tilde{\mathcal{H}}$, in which operators on each site have been replaced by their projections, $\tilde{\mathcal{O}} = \mathcal{P}_{\frac{3}{2}} \mathcal{O} \mathcal{P}_{\frac{3}{2}}$, where $\mathcal{P}_{\frac{3}{2}}$ is the

Table 2 A list of representative ordered double perovskites in which the magnetic ions have d^1 or d^2 electron configuration[a]

Compound	B'	Electron configuration	Θ_{CW} (K)	μ_{eff} (μ_B)	Magnetic transition	References
Ba_2YMoO_6	Mo^{5+}	$4d^1$	$-91 \sim -219$	$1.34 \sim 1.72$	PM down to 2 K	33–38
Sr_2MgReO_6	Re^{6+}	$5d^1$	-426	1.72	spin glass, $T_G \sim 50$ K	40
Ba_2NaOsO_6	Os^{7+}	$5d^1$	~ -10	~ 0.6	FM $T_c = 6.8$ K	44
Ba_2CaOsO_6	Os^{6+}	$5d^2$	-157	1.61	AF $T_c = 51$ K	42
La_2LiReO_6	Re^{5+}	$5d^2$	-204	1.97	PM down to 2 K	39

[a]Variations in the Curie-Weiss temperature Θ_{CW} and effective magnetic moment μ_{eff} may originate from the experimental fitting of data at different temperature ranges.

Abbreviations: AF, antiferromagnetic; FM, ferromagnetic; PM, paramagnetic; T_c, ordering temperature; T_G, glass transition temperature.

projection operator onto the $J_{\text{eff}} = 3/2$ multiplet. Some algebra shows that these projections are quite nontrivial:

$$\tilde{S}^{\alpha}_{i,xy} = \frac{1+2\delta_{\alpha,z}}{4} S^{\alpha}_i - \frac{1}{3} S^z_i S^{\alpha}_i S^z_i \quad (\alpha = x, y, z), \quad \tilde{n}_{i,xy} = \frac{3}{4} - \frac{1}{3}\left(S^z_i\right)^2, \qquad 8.$$

where $\boldsymbol{S}_i$ is the final projected $J_{\text{eff}} = 3/2$ effective spin. Spin and occupation number operators for other orbitals can be readily generated by a cubic permutation.

The quadratic and cubic products of S^{μ}_i represent components of the quadrupolar and octupolar tensors, respectively. We see that the innocuous-looking Hamiltonian in Equation 7 is transformed, after the strong SOC projection using $\mathcal{O} \to \tilde{\mathcal{O}}$ via Equation 8, into a highly nontrivial interaction with octupolar and quadrupolar couplings of the same order as ordinary bilinear exchange. This mechanism generating higher-orderspin exchange is quite generic and applies equally to all the interactions in a typical strong SOC situation. It gives access to a variety of exotic physics of multipolar systems (125, 153).

For the d^1 double perovskites, two natural additional exchange channels were identified between nearest neighbors in Reference 54: a ferromagnetic exchange, J', between orthogonal orbitals and an electrostatic quadrupole interaction, V. Details of these interactions can be found in Reference 54. Similar considerations apply to the d^2 case, as described in Reference 55. All the interactions in both cases become multipolar in character after the strong SOC projection.

3.1.3. Mean-field theory. With the exotic interaction Hamiltonians discussed above, unusual phases are expected even in a mean-field treatment. We explore this here and subsequently consider the possibility of phases beyond mean-field theory. The Weiss mean-field treatment consists, as usual, of decoupling the interactions between sites to generate self-consistent single-site problems. As a result of the multipolar interactions, each single-site Hamiltonian contains not only an effective Zeeman field but also effective quadrupolar and octupolar anisotropies. The latter define additional multipolar order parameters in the mean-field theory. A full analysis is given in Reference 54 for the d^1 case and Reference 55 for the d^2 case. We summarize only the former as an example.

A representative cut through the three-dimensional phase diagram is depicted in **Figure 7**. At zero temperature, three phases appear, all with nominally conventional ferromagnetic or AF dipolar magnetic order. However, there are unconventional aspects revealed upon closer inspection.

The simplest state is the AF phase, appearing for small J'/J and V/J. It has a conventional two-sublattice structure, with states on either sublattice related by time reversal. However, although it

displays local static dipole moments, their magnitude is small and in fact vanishes as temperature $T \to 0$. This is particularly surprising in a mean-field theory (for a conventional Heisenberg system, mean-field theory gives a full moment). In fact, accompanying the dipole moment is a large staggered octupole moment, which competes with and substantially suppresses the dipolar order.

With larger J'/J and V/J, the system develops ferromagnetic phases, FM110 and FM100, with net ferromagnetic moments along [110] and [100] directions, respectively. These two nonuniform ferromagnets are rather unconventional, as they actually have a two-sublattice structure with partial cancellation of nonparallel magnetic moments in the ferromagnetic magnetization. In fact, the two-sublattice structure is a manifestation of staggered quadrupolar order, and it is this quadrupolar ordering that predominantly drives the formation of these two phases. The magnetism develops atop it. Because orbital polarization is distinct on the two sublattices, they cannot be time-reversal conjugates, and consequently when magnetism onsets, a net ferromagnetic moment results.

The driving role of the quadrupolar order can be seen from the $T > 0$ phase diagram. Over a wide range of intermediate temperature, the ferromagnetic order is destroyed, with the FM region (and part of the AF one) being replaced by a purely quadrupolar ordered phase. In the quadrupolar phase, TRS is unbroken, which is sufficient to require the dipolar and octupolar order parameters to vanish. A standard classification scheme for quadrupolar states is to examine the eigenvalues of the traceless quadrupolar tensor $Q_i^{\mu\nu} = \langle S_i^\mu S_i^\nu \rangle - \frac{1}{3} S(S+1)\delta^{\mu\nu}$, where the eigenvalues must sum to zero (here $S = 3/2$ for d^1). The quadrupolar phase with only one independent eigenvalue, i.e., eigenvalues $(Q) = \{q, q, -2q\}$, is called the uniaxial nematic phase and corresponds to the situation in which one principal axis is distinguished from the other two that remain equivalent. This type of spin nematic has been studied theoretically in $S = 1$ Heisenberg models with strong biquadratic interactions (120), although it is hard to achieve such strong biquadratic exchange in conventional systems. In the most general case, there may be two independent

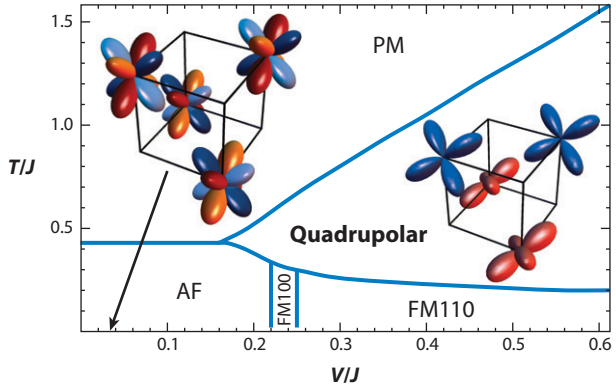

Figure 7

A cut of the mean-field phase diagram for d^1 double perovskites at fixed $J' = 0.2\,J$ as a function of temperature, T, and electric quadrupole interaction, V. The antiferromagnetic (AF) state is illustrated at $T = 0$ by an image of the orbital wave functions for $S^x = +1/2$ (*with positive and negative regions colored blue and light blue, respectively*) and for the $S^x = -1/2$ (*with positive and negative regions colored red and orange, respectively*). In the quadrupolar state, the charge density is shown. The FM110 and FM100 are ferromagnetic states with net magnetization along the [110] and [100] axes (and spin-orbital entanglement, which is difficult to illustrate). The curves are obtained from calculations in Reference 54. Abbreviation: FM, ferromagnetic; PM, paramagnetic.

eigenvalues, i.e., eigenvalues $(Q) = \{q_1, q_2, -q_1 - q_2\}$, with $q_1 \neq q_2$. This is called a biaxial nematic phase, and all three principal axes are nonequivalent. The quadrupolar state obtained here is such a biaxial nematic phase.

Such a quadrupolar phase also exists in the phase diagram for the d^2 double perovskites (55) but in that case appears even at $T = 0$. This difference between the d^1 and d^2 cases occurs because within Weiss mean-field theory, a Kramers ion, such as d^1, must always break TRS at $T = 0$ to avoid ground-state degeneracy.

3.1.4. Beyond mean-field theory. As remarked earlier, multipolar interactions tend to destabilize conventional, magnetically ordered semiclassical ground states. Roughly speaking, this is because they contain many more spin-flip terms analogous to the $S_i^+ S_j^-$ couplings, which are part of the usual Heisenberg two-spin interactions. Quantum disordered ground states can be established rigorously for AKLT models (121), which have specially tuned $SU^{(2)}$ invariant Hamiltonians that can be written entirely in terms of a positive semidefinite sum of projection operators. They can also be found in a controlled manner for large N models with enlarged SU(N) or Sp(N) symmetry (122). Neither approach can be directly applied here, but it is clear that the multipolar Hamiltonians that occur naturally for d^1 and d^2 systems are somewhat intermediate between conventional spin models and these special cases. Thus, in frustrated geometries, quantum disordered states may occur.

A simple way to check for disordered states is to gauge the magnitude of quantum fluctuations within a spin-wave expansion (generalized for multipolar phases) around the mean-field states. Indeed, using a generalized Holstein-Primakoff spin-wave theory, we find that quantum fluctuations are strong when J'/J and V/J are small (54). This strongly points to effects beyond mean field and to the likelihood of a nonmagnetic ground state. By examining various limits, both valence bond solid and quantum spin liquid states were proposed in Reference 54 for this region of the phase diagram of the d^1 systems. Further quantitative study of models of this type would be highly desirable, but this is challenging and probably requires at least significant extension of existing numerical methods.

Other theoretical work has considered the effects of noncubic crystal fields, which split the quadruplet ground state to form a low-energy doublet. This then reduces to an effective $S = 1/2$ model but with highly anisotropic interactions, with anisotropy depending on the bond orientation. The resulting exchange model may be strongly frustrated. In such cases, quantum fluctuations may also support a quantum spin liquid phase (56), which is amenable to analysis by more conventional methods.

3.1.5. Connections to experiments. A detailed discussion about the applications of theory to experiments, and on specific materials, can be found in References 54 and 55. Here we comment on a few examples for which strong SOC phenomenology is most compelling. In general, for the strong SOC limit to apply, both noncubic crystal fields and exchange interactions should be small compared with the spin-orbit splitting. The latter is of order 100 meV for 4*d* materials, such as Mo^{5+}, and a few times larger for the 5*d* materials. This is quite large compared with exchange interactions in double perovskites but not necessarily large compared with crystal field perturbations in noncubic crystals. Thus, we focus on cases in which elastic X-ray scattering measurements find a cubic structure. This presumably indicates the absence of a static Jahn-Teller effect, although the dynamic or nonuniform effects of Jahn-Teller phonon coupling may still be important.

We have already mentioned Ba_2YMoO_6, which remains cubic at low temperatures and has a magnetic entropy approximately equal to R ln 4, which is consistent with a $J_{\text{eff}} = 3/2$ local moment (34). This material avoids any apparent phase transitions down to 2 K, despite rather

strong AF interactions. An energy gap is indicated in recent NMR and inelastic neutron-scattering measurements, which may be associated with valence bond formation (36). An unusual feature seen in this material, which occurs in a number of double perovskites, is the existence of two Curie regimes in the magnetic susceptibility: above 100 K and below 50 K (34, 35, 37). This is suggestive of some single-ion anisotropy, which would explain the existence of two Curie regimes because it splits the fourfold degeneracy of the $J_{\rm eff} = 3/2$ states but leaves a twofold Kramers doublet at temperatures below 50 K, which still gives a Curie signal. This could perhaps be associated with quadrupolar order or with a lattice-driven distortion. The macroscopic cubic symmetry appears at odds with the latter, but a set of random local distortions with statistical cubic symmetry might be a possibility. More recent experiments have observed the emergence of an additional phonon mode below 130 K, which is consistent with a local structural change (37).

A second example is Ba_2NaOsO_6, for which the ground state below 6.8 K was found to be ferromagnetic with an easy axis along the [110] direction (44). The [110] easy axis is quite unusual and indeed does not occur in standard Landau theory for ferromagnets, in which weak cubic anisotropy (quartic terms) always selects either a [100] or [111] axis. This is an indication for the validity of the strong SOC description, which indeed predicts [110] ferromagnetism to be dominant because of the quadrupolar mechanism. Experimental confirmation requires measurement of a structural change associated to the quadrupolar ordering, which so far has not been observed. However, several other indications are in favor of quadrupolar ordering (54).

4. CONCLUDING REMARKS AND OUTLOOK

The investigation of correlated electron systems with strong SOC is still in its infancy. In this review, we summarized and explained recent developments in theoretical and experimental research in this rapidly growing area. We showed that SOC tends to act with Coulomb interactions to enhance the degree of electron correlations, producing spin-orbit-assisted Mott insulators. In the weak-to-intermediate correlation regime, we described possible electronic states with topological band structures. When correlations are strong enough that a local moment description applies, we discussed how spin liquid and multipolar phases may occur due to spin-orbital entanglement. We explored possible applications to pyrochlore iridates in the weak-to-intermediate correlation regime, and honeycomb iridates and double perovskites with $4d/5d$ transition metal elements in the strong Mott regime. Because of space limitations, many important systems were not discussed in this review. This includes the Ruddlesden-Popper series of perovskite iridates (9–16, 154, 155) $Sr_{n+1}Ir_nO_{3n+1}$, whose $n = \infty, 1, 2$ members are some of the most investigated materials in this class. In particular, Sr_2IrO_4 warrants special attention as an approximate homolog of the parent material of some of the high-T_c cuprates La_2CuO_4. As with La_2CuO_4, Sr_2IrO_4 is an AF insulator (9–13) with a very large exchange constant of $J \sim 700$–1000 K (11–13), which is somewhat smaller than but comparable to that of the cuprates, and a charge gap of $\Delta_c \sim 350$–650 meV or $4000-7500$ K, many times larger than J. Both Sr_2IrO_4 and $Sr_3Ir_2O_7$ have served as striking examples of the power of modern RIXS, which is remarkably suited for $5d$ compounds (10–16). RIXS has provided a direct probe of spin and orbital states and dynamics. By RIXS, it has been possible to test and confirm the $J_{\rm eff} = 1/2$ character of the Ir^{4+} state in Sr_2IrO_4 (10) and to measure the full spin-wave dispersion in both compounds (11–16). Such measurements reinforce the analogy of Sr_2IrO_4 to the cuprates and have motivated a strong push to dope this material (126–128) in hopes of finding high-temperature superconductivity, pseudogap behavior, etc., as also suggested theoretically (129). This program is underway, although at the time of this writing superconductivity has not been found.

In general, doping of correlated insulators with strong SOC is a very interesting subject. In the traditional venue, the Mott metal-insulator quantum phase transition may be tuned either by

bandwidth control at fixed stoichiometric filling or by filling control, and these two types of Mott transitions have distinct characters (2). In this review, we have already remarked upon the seemingly distinct behavior of the bandwidth-controlled transition (and the thermal transition at fixed filling) in the strong SOC regime from the usual strong first-order transition in 3*d* transition metal compounds. It may be that the filling-controlled transitions are also qualitatively different in the strong SOC case. There is very little theoretical work on this problem (129–131), which promises to be a rich subject for future study and not only in Sr_2IrO_4.

Another important topic that has been mentioned but not given in-depth attention in this review is the emergence of fractionalized exotic phases from topological bands. This possibility is vetted experimentally and theoretically by the most-studied fractionalized states of matter, the fractional quantum Hall effect (FQHE) state of two-dimensional electron gases in high magnetic fields. The Landau levels of that problem can be viewed as the simplest examples of bands with a nontrivial Chern number, and it is understood that the FQHE originates from interacting electrons that partially fill a Landau level. Many theorists have suggested that FQHE can occur because of fractionally filled bands with a nontrivial Chern number in crystalline materials with broken TRS: a fractional Chern insulator (72–74). Time-reversal symmetric fractional TIs (132–134) have also been proposed in both 2D and 3D, as have other fractionalized phases, such as the topological Mott insulator (8, 53). Although current theoretical understanding demonstrates clearly that all these phases may exist, i.e., that they are stable phases of matter for some Hamiltonian parameters, they are all outside the domain of conventional mean-field approaches, including those combined with ab initio methods, such as LDA+U and DMFT. For many of the other phases described in this review, however, mean-field approaches are adequate.

Also beyond these mean-field approaches are numerous possible quantum critical points (as well as thermal ones). The rich variety of phases found already in the studies discussed in this review implies that suitable phase transitions between these phases should be accessible. This includes, of course, MITs but also transitions to the onset of magnetic order and between different types of band topology. In many experimental systems with weak SOC, quantum criticality is seen to coincide with unconventional superconductivity, and many believe the former is a causative factor in the latter (135). It will be very interesting to seek superconductivity from quantum critical fluctuations in strong SOC materials, and if it exists, to see whether topological superconductivity might result. Experimentally, strong SOC tightens the link between electronic and lattice structure so that a very strong influence of pressure/strain may be expected in these materials. We anticipate a growing number of studies of criticality in this class of systems.

As in any developing field, there are controversies. The $J_{\text{eff}} = 1/2$ limit is actively debated in different iridates. The degree of spin-orbital entanglement can be addressed by several distinct experiments and should vary from material to material, depending upon the strength of crystal fields, the electron bandwidth, the onsite electron repulsion, and other factors. Although the $J_{\text{eff}} = 1/2$ picture is appealing and simple, it is probably not essential to many of the phenomena we have discussed. Also at issue is the nature of the correlated insulating state. Some authors distinguish between Mott and Slater insulators, with insulating behavior being due to magnetic order in the latter. It is not clear whether this distinction is well defined, especially at zero temperature, given that magnetic order itself can arise only from Coulomb interactions. In general, there is no reason to have a phase transition if the magnetic ordering pattern is unchanged, as the interaction strength is increased up to the local moment regime. Different experiments (136, 137) that try to differentiate the two may be formulated: Is the system conducting or insulating above the magnetically ordering temperature? Is the charge gap Δ_c large compared with the exchange J? Is the MIT continuous or first order? These criteria need not agree. A related issue is the degree of correlation in, for example, iridates, with presumably Slater insulators being less correlated. This question is typically posed by ab

initio–based approaches, such as LDA+U combined with DMFT. We remark that via these techniques even the correlation strength of high-T_c cuprates might be questioned (138), so the physical significance of this debate is opaque to us. Finally, the strong SOC limit itself is open to question. The strong SOC limit indeed depends not only on the ratio of SOC to noncubic crystal fields but also on the strength of hopping or exchange relative to SOC. Mazin et al. (139) have suggested that SOC is not critical to the insulating state in Na_2IrO_3 (140, 156).

Moving beyond these debates, perhaps one of the most ambitious programs for the future is the engineering of desired electronic states. An appealing possibility is combining the materials discussed in this review with advances in layer-by-layer atomic growth of oxides to produce designer heterostructures of iridates and other strong SOC systems. For example, various heterostructures of perovskites (141, 142) (including SrIrO3) as well as of $R_2Ir_2O_7$ along the [111] direction (143) have been proposed, and several nontrivial phases, such as TIs and quantum Hall states, are predicted to exist under certain conditions. Experiments of this type are within the realm of possibility in the near future.

At the time of writing, the materials synthesis and experimental characterization of diverse 4*d* and 5*d* transition metal oxides is only increasing. The effects of carrier doping, hydrostatic pressure, and high magnetic fields are under investigation. The outcome of these experiments and existing and future theory may uncover entirely new classes of many-body quantum ground states in strongly spin-orbit coupled systems.

DISCLOSURE STATEMENT

The authors are not aware of any affiliations, memberships, funding, or financial holdings that might be perceived as affecting the objectivity of this review.

ACKNOWLEDGMENTS

We thank S. Bhattacharjee, A. Burkov, R. Chen, A. Go, M. Hermele, G.S. Jeon, E.K.H. Lee, E.-G. Moon, D. Pesin, K. Park, L. Savary, C. Xu, and B.-J. Yang for collaboration on work related to this review and for helpful discussions. We are also grateful to H.D. Drew, P. Gegenwart, B.J. Kim, Y.-J. Kim, S.R. Julian, S. Nakatsuji, R. Perry, Y. Singh, A.B. Sushkov, and H. Takagi for sharing their experimental data and fruitful discussions. Our special thanks go to J.J. Ishikawa, S. Nakatsuji, and D.E. MacLaughlin for providing the plot used in **Figure 4*a***. This work was supported by the Walter Sumner Foundation (WWK), DOE award number DE-SC0003910 (GC), NSERC, CIFAR, Center for Quantum Materials at the University of Toronto (YBK), and NSF grant number DMR–1206809 and DOE Basic Energy Sciences Grant number DE-FG02-08ER46524 (LB). Some of this work was carried out at the KITP and funded by NSF grant PHY-1125915. Research at Perimeter Institute is supported by the Government of Canada through Industry Canada and by the Province of Ontario through the Ministry of Research & Innovation.

LITERATURE CITED

1. Mott NF. 1990. *Metal-Insulator Transitions*. London: Taylor & Francis
2. Imada M, Fujimori A, Tokura Y. 1998. *Rev. Mod. Phys.* 70:1039–263
3. Santini P, Carretta S, Amoretti G, Caciuffo R, Magnani N, Lander GH. 2009. *Rev. Mod. Phys.* 81:807–63
4. Hasan MZ, Kane CL. 2010. *Rev. Mod. Phys.* 82:3045–67
5. Qi X-L, Zhang S-C. 2011. *Rev. Mod. Phys.* 83:1057–110
6. Hasan MZ, Moore JE. 2011. *Annu. Rev. Condens. Matter Phys.* 2:55–78

7. Georges A, Medici LD, Mravlje J. 2013. *Annu. Rev. Condens. Matter Phys.* 4:137–78
8. Pesin D, Balents L. 2010. *Nat. Phys.* 6:376–81
9. Kim BJ, Jin H, Moon SJ, Kim J-Y, Park B-G, et al. 2008. *Phys. Rev. Lett.* 101:076402
10. Kim BJ, Ohsumi H, Komesu T, Sakai S, Morita T, et al. 2009. *Science* 323:1329–32
11. Fujiyama S, Ohsumi H, Komesu T, Matsuno J, Kim BJ, et al. 2012. *Phys. Rev. Lett.* 108:247212
12. Kim J, Casa D, Upton MH, Gog T, Kim Y-J, et al. 2012. *Phys. Rev. Lett.* 108:177003
13. Kim JW, Choi Y, Kim J, Mitchell JF, Jackeli G, et al. 2012. *Phys. Rev. Lett.* 109:037204
14. Kim J, Said AH, Casa D, Upton MH, Gog T, et al. 2012. *Phys. Rev. Lett.* 109:157402
15. Fujiyama S, Ohashi K, Ohsumi H, Sugimoto K, Takayama T, et al. 2012. *Phys. Rev. B* 86:174414
16. King PDC, Takayama T, Tamai A, Rozbicki E, McKeown Walker S, et al. 2013. *Phys. Rev. B* 87:241106
17. Singh Y, Gegenwart P. 2010. *Phys. Rev. B* 82:064412
18. Singh Y, Manni S, Reuther J, Berlijn T, Thomale R, et al. 2012. *Phys. Rev. Lett.* 108:127203
19. Gretarsson H, Clancy JP, Liu X, Hill JP, Bozin E, et al. 2013. *Phys. Rev. Lett.* 110:076402
20. Liu X, Berlijn T, Yin W-G, Ku W, Tsvelik A, et al. 2011. *Phys. Rev. B* 83:220403
21. Clancy JP, Chen N, Kim CY, Chen WF, Plumb KW, et al. 2012. *Phys. Rev. B* 86:195131
22. Choi SK, Coldea R, Kolmogorov AN, Lancaster T, Mazin II, et al. 2012. *Phys. Rev. Lett.* 108:127204
23. Yanagishima D, Maeno Y. 2001. *J. Phys. Soc. Jpn.* 70:2880–83
24. Matsuhira K, Wakeshima M, Nakanishi R, Yamada T, Nakamura A, et al. 2007. *J. Phys. Soc. Jpn.* 76:043706
25. Qi TF, Korneta OB, Wan X, DeLong LE, Schlottmann P, Cao G. 2012. *J. Phys. Condens. Matter* 24:345601
26. Okamoto Y, Nohara M, Aruga-Katori H, Takagi H. 2007. *Phys. Rev. Lett.* 99:137207
27. Kuriyama H, Matsuno J, Niitaka S, Uchida M, Hashizume D, et al. 2010. *Appl. Phys. Lett.* 96:182103
28. Shi YG, Guo YF, Yu S, Arai M, Belik AA, et al. 2009. *Phys. Rev. B* 80:161104
29. Yamaura J, Ohgushi K, Ohsumi H, Hasegawa T, Yamauchi I, et al. 2012. *Phys. Rev. Lett.* 108:247205
30. Krimmel A, Mücksch M, Tsurkan V, Koza MM, Mutka H, Loidl A. 2005. *Phys. Rev. Lett.* 94:237402
31. Büttgen N, Zymara A, Kegler C, Tsurkan V, Loidl A. 2006. *Phys. Rev. B* 73:132409
32. Chen G, Balents L, Schnyder AP. 2009. *Phys. Rev. Lett.* 102:096406
33. Cussen EJ, Lynham DR, Rogers J. 2006. *Chem. Mater.* 18:2855–66
34. de Vries MA, Mclaughlin AC, Bos J-WG. 2010. *Phys. Rev. Lett.* 104:177202
35. Aharen T, Greedan JE, Bridges CA, Aczel AA, Rodriguez J, et al. 2010. *Phys. Rev. B* 81:224409
36. Carlo JP, Clancy JP, Aharen T, Yamani Z, Ruff JPC, et al. 2011. *Phys. Rev. B* 84:100404
37. Qu Z, Zou Y, Zhang S, Ling L, Zhang L, Zhang Y. 2013. *J. Appl. Phys.* 113:17E137
38. de Vries MA, Piatek JO, Misek M, Lord JS, Ronnow HM, Bos J-WG. 2013. *New J. Phys.* 15:043024
39. Aharen T, Greedan JE, Bridges CA, Aczel AA, Rodriguez J, et al. 2010. *Phys. Rev. B* 81:064436
40. Wiebe CR, Greedan JE, Kyriakou PP, Luke GM, Gardner JS, et al. 2003. *Phys. Rev. B* 68:134410
41. Wiebe CR, Greedan JE, Luke GM, Gardner JS. 2002. *Phys. Rev. B* 65:144413
42. Yamamura K, Wakeshima M, Hinatsu Y. 2006. *J. Solid State Chem.* 179:605–12
43. Stitzer KE, Smith MD, zur Loye H-C. 2002. *Solid State Sci.* 4:311–18
44. Erickson AS, Misra S, Miller GJ, Gupta RR, Schlesinger Z, et al. 2007. *Phys. Rev. Lett.* 99:016404
45. Steele AJ, Baker PJ, Lancaster T, Pratt FL, Franke I, et al. 2011. *Phys. Rev. B* 84:144416
46. Aharen T, Greedan JE, Ning F, Imai T, Michaelis V, et al. 2009. *Phys. Rev. B* 80:134423
47. Wan X, Turner AM, Vishwanath A, Savrasov SY. 2011. *Phys. Rev. B* 83:205101
48. Witczak-Krempa W, Kim YB. 2012. *Phys. Rev. B* 85:045124
49. Burkov AA, Balents L. 2011. *Phys. Rev. Lett.* 107:127205
50. Wan X, Vishwanath A, Savrasov SY. 2012. *Phys. Rev. Lett.* 108:146601
51. Go A, Witczak-Krempa W, Jeon GS, Park K, Kim YB. 2012. *Phys. Rev. Lett.* 109:066401
52. Yang B-J, Kim YB. 2010. *Phys. Rev. B* 82:085111
53. Witczak-Krempa W, Choy TP, Kim YB. 2010. *Phys. Rev. B* 82:165122
54. Chen G, Pereira R, Balents L. 2010. *Phys. Rev. B* 82:174440
55. Chen G, Balents L. 2011. *Phys. Rev. B* 84:094420
56. Dodds T, Choy T-P, Kim YB. 2011. *Phys. Rev. B* 84:104439

57. Mong RSK, Essin AM, Moore JE. 2010. *Phys. Rev. B* 81:245209
58. Turner AM, Zhang Y, Mong RSK, Vishwanath A. 2012. *Phys. Rev. B* 85:165120
59. Hughes TL, Prodan E, Bernevig BA. 2011. *Phys. Rev. B* 83:245132
60. Fang C, Gilbert MJ, Bernevig BA. 2013. *Phys. Rev. B* 88:085406
61. Wang Z, Qi X-L, Zhang S-C. 2010. *Phys. Rev. Lett.* 105:256803
62. Wang Z, Qi X-L, Zhang S-C. 2012. *Phys. Rev. B* 85:165126
63. Wang Z, Zhang S-C. 2012. *Phys. Rev. X* 2:031008
64. Volovik GA. 2003. *The Universe in a Helium Droplet*. Oxford: Oxford Univ. Press
65. Haldane FD. 2004. *Phys. Rev. Lett.* 93:206602
66. Nielsen H, Ninomiya M. 1983. *Phys. Lett. B* 130:389–96
67. Xu G, Weng H, Wang Z, Dai X, Fang Z. 2011. *Phys. Rev. Lett.* 107:186806
68. Halász GB, Balents L. 2012. *Phys. Rev. B* 85:035103
69. Meng T, Balents L. 2012. *Phys. Rev. B* 86:054504
70. Turner AM, Vishwanath A. 2013. arXiv preprint arXiv:1301.0330
71. Vafek O, Vishwanath A. 2014. *Annu. Rev. Condens. Matter Phys.* 5:83–112
72. Sheng DN, Gu Z-C, Sun K, Sheng L. 2011. *Nat. Commun.* 2:389
73. Neupert T, Santos L, Chamon C, Mudry C. 2011. *Phys. Rev. Lett.* 106:236804
74. Tang E, Mei J-W, Wen X-G. 2011. *Phys. Rev. Lett.* 106:236802
75. Machida Y, Nakatsuji S, Onoda S, Tayama T, Sakakibara T. 2009. *Nature* 463:210–13
76. Taira N, Wakeshima M, Hinatsu Y. 2001. *J. Phys Condens. Matter* 13:5527
77. Fukazawa H, Maeno Y. 2002. *J. Phys. Soc. Jpn.* 71:2578–79
78. Matsuhira K, Wakeshima M, Hinatsu Y, Takagi S. 2011. *J. Phys. Soc. Jpn.* 80:094701
79. Hasegawa T, Ogita N, Matsuhira K, Takagi S, Wakeshima M, et al. 2010. *J. Phys. Conf. Ser.* 200:012054
80. Zhao S, Mackie JM, MacLaughlin DE, Bernal OO, Ishikawa JJ, et al. 2011. *Phys. Rev. B* 83:180402
81. Ishikawa JJ, O'Farrell ECT, Nakatsuji S. 2012. *Phys. Rev. B* 85:245109
82. Tomiyasu K, Matsuhira K, Iwasa K, Watahiki M, Takagi S, et al. 2012. *J. Phys. Soc. Jpn.* 81:034709
83. Tafti FF, Ishikawa JJ, McCollam A, Nakatsuji S, Julian SR. 2012. *Phys. Rev. B* 85:205104
84. Sakata M, Kagayama T, Shimizu K, Matsuhira K, Takagi S, et al. 2011. *Phys. Rev. B* 83:041102
85. Shapiro MC, Riggs SC, Stone MB, de la Cruz CR, Chi S, et al. 2012. *Phys. Rev. B* 85:214434
86. Disseler SM, Dhital C, Hogan TC, Amato A, Giblin SR, et al. 2012. *Phys. Rev. B* 85:174441
87. Guo H, Matsuhira K, Kawasaki I, Wakeshima M, Hinatsu Y, et al. 2013. *Phys. Rev. B* 88:060411
88. Disseler SM, Dhital C, Amato A, Giblin SR, de la Cruz C, et al. 2012. *Phys. Rev. B* 86:014428
89. Sagayama H, Uematsu D, Arima T, Sugimoto K, Ishikawa JJ, et al. 2013. *Phys. Rev. B* 87:100403
90. Subramanian M, Aravamudan G, Rao GS. 1983. *Prog. Solid State Chem.* 15:55–143
91. Koo H-J, Whangbo M-H, Kennedy B. 1998. *J. Solid State Chem.* 136:269–73
92. Witczak-Krempa W, Go A, Kim YB. 2013. *Phys. Rev. B* 87:155101
93. Kurita M, Yamaji Y, Imada M. 2011. *J. Phys. Soc. Jpn.* 80:044708
94. Moon E-G, Xu C, Kim YB, Balents L. 2012. arXiv preprint arXiv:1212.1168
95. Yang K-Y, Lu Y-M, Ran Y. 2011. *Phys. Rev. B* 84:075129
96. Nielsen HB, Ninomiya M. 1983. *Phys. Lett. B* 130:389–96
97. Kotliar G, Savrasov SY, Haule K, Oudovenko VS, Parcollet O, Marianetti CA. 2006. *Rev. Mod. Phys.* 78:865–951
98. Maier T, Jarrell M, Pruschke T, Hettler MH. 2005. *Rev. Mod. Phys.* 77:1027–80
99. Nakatsuji S, Machida Y, Maeno Y, Tayama T, Sakakibara T, et al. 2006. *Phys. Rev. Lett.* 96:087204
100. Machida Y, Nakatsuji S, Maeno Y, Tayama T, Sakakibara T, Onoda S. 2007. *Phys. Rev. Lett.* 98:057203
101. Onoda S, Tanaka Y. 2010. *Phys. Rev. Lett.* 105:047201
102. Onoda S, Tanaka Y. 2011. *Phys. Rev. B* 83:094411
103. Flint R, Senthil T. 2013. *Phys. Rev. B* 87:125147
104. Chen G, Hermele M. 2012. *Phys. Rev. B* 86:235129
105. Ueda K, Fujioka J, Takahashi Y, Suzuki T, Ishiwata S, et al. 2012. *Phys. Rev. Lett.* 109:136402
106. Kin-Ho Lee E, Bhattacharjee S, Kim YB. 2012. *Phys. Rev. B* 87:214416

107. Kugel KI, Khomskii DI. 1982. *Sov. Phys. Usp.* 25:231–56
108. Jahn H, Teller E. 1937. *Proc. R. Soc. Lond. A* 161:220–35
109. Jackeli G, Khaliullin G. 2009. *Phys. Rev. Lett.* 102:017205
110. Kitaev A. 2006. *Ann. Phys.* 321:2–111
111. Chaloupka J, Jackeli G, Khaliullin G. 2010. *Phys. Rev. Lett.* 105:027204
112. Chaloupka J, Jackeli G, Khaliullin G. 2013. *Phys. Rev. Lett.* 110:097204
113. Chen G, Balents L. 2008. *Phys. Rev. B* 78:094403
114. Mazin II, Jeschke HO, Foyevtsova K, Valentí R, Khomskii DI. 2012. *Phys. Rev. Lett.* 109:197201
115. Reuther J, Thomale R, Trebst S. 2011. *Phys. Rev. B* 84:100406
116. Kimchi I, You Y-Z. 2011. *Phys. Rev. B* 84:180407
117. Bhattacharjee S, Lee S-S, Kim YB. 2012. *New J. Phys.* 14:073015
118. Reuther J, Thomale R, Rachel S. 2012. *Phys. Rev. B* 86:155127
119. Goodenough JB. 1968. *Phys. Rev.* 171:466
120. Läuchli A, Mila F, Penc K. 2006. *Phys. Rev. Lett.* 97:087205
121. Affleck I, Kennedy T, Lieb E, Tasaki H. 1988. *Commun. Math. Phys.* 115:477–528
122. Sachdev S. 2003. *Ann. Henri Poincaré* 4:637
123. Lee KW, Pickett W. 2007. *Europhys. Lett.* 80:37008
124. Xiang HJ, Whangbo M-H. 2007. *Phys. Rev. B* 75:052407
125. Shiina R, Sakai O, Shiba H, Thalmeier P. 1998. *J. Phys. Soc. Jpn.* 67:941–49
126. Korneta OB, Qi T, Chikara S, Parkin S, De Long LE, et al. 2010. *Phys. Rev. B* 82:115117
127. Qi TF, Korneta OB, Li L, Butrouna K, Cao VS, et al. 2012. *Phys. Rev. B* 86:125105
128. Calder S, Cao G-X, Lumsden MD, Kim JW, Gai Z, et al. 2012. *Phys. Rev. B* 86:220403
129. Wang F, Senthil T. 2011. *Phys. Rev. Lett.* 106:136402
130. Okamoto S. 2013. *Phys Rev Lett.* 110:066403
131. You Y-Z, Kimchi I, Vishwanath A. 2012. *Phys. Rev. B* 86:085145
132. Levin M, Stern A. 2009. *Phys. Rev. Lett.* 103:196803
133. Maciejko J, Qi X-L, Karch A, Zhang S-C. 2012. *Phys. Rev. B* 86:235128
134. Swingle B, Barkeshli M, McGreevy J, Senthil T. 2011. *Phys. Rev. B* 83:195139
135. Coleman P, Schofield AJ. 2005. *Nature* 433:226–29
136. Comin R, Levy G, Ludbrook B, Zhu Z-H, Veenstra CN, et al. 2012. *Phys. Rev. Lett.* 109:266406
137. Hsieh D, Mahmood F, Torchinsky D, Cao G, Gedik N. 2012. *Phys. Rev. B* 86:035128
138. de' Medici L, Wang X, Capone M, Millis AJ. 2009. *Phys. Rev. B* 80:054501
139. Mazin I, Manni S, Foyevtsova K, Jeschke HO, Gegenwart P, Valenti R. 2013. arXiv preprint arXiv: 1304.2258
140. Foyevtsova K, Jeschke HO, Mazin I, Khomskii D, Valenti R. 2013. *Phys. Rev. B* 88:035107
141. Xiao D, Zhu W, Ran Y, Nagaosa N, Okamoto S. 2011. *Nat. Commun.* 2:596
142. Wang F, Ran Y. 2011. *Phys. Rev. B* 84:241103
143. Hu X, Rüegg A, Fiete GA. 2012. *Phys. Rev. B* 86:235141
144. Jackeli G, Khaliullin G. 2009. *Phys. Rev. Lett.* 103:067205
145. Chen G, Schnyder A, Balents L. 2009. *Phys. Rev. B* 80:224209
146. Wang C, Potter AC, Senthil T. 2013. *Phys. Rev. B* 88:115137
147. Metlitski MA, Kane CL, Fisher MPA. 2013. arXiv:1306.3286 [cond-mat.st-el]
148. Fidknowski L, Chen X, Vishwanath A. 2013. *Phys. Rev. X* 3:041016
149. Bonderson P, Nayak C, Qi X-L. 2013. *J. Stat. Mech.* 2013:P09016
150. Kargarian M, Fiete GA. 2013. *Phys. Rev. Lett.* 110:156403
151. Kargarian M, Wen J, Fiete GA. 2011. *Phys. Rev. B* 83:165112
152. Lee S, Paramekanti A, Kim YB. 2013. arXiv:1305.0827 [cond-mat.str-el]
153. Santini P, Carretta S, Amoretti G, Caciuffo R, Magnani N, Lander GH. 2009. *Rev. Mod. Phys.* 81:807–63
154. Carter JM, Kee H-Y. 2013. *Phys. Rev. B* 87:014433
155. Zeb MA, Kee HY. 2012. *Phys. Rev. B* 86:085149
156. Foyevtsova K, Jeschke O, Mazin I, Khomskii D, Valenti R. 2013. arXiv:1303.2105

Annual Review of Condensed Matter Physics

Volume 5, 2014

Contents

Errata

An online log of corrections to *Annual Review of Condensed Matter Physics* articles may be found at http://www.annualreviews.org/errata/conmatphys